Report of the National Research Center for Disaster Prevention, No. 39, March 1987

550.34(521.2/.6)

Examination of the NRCDP's (The National Research Center for Disaster Prevention) Seismic Observational Network as regards I. Detectability-locatability II. Accuracy of the determination of earthquake source parameters

By

Dimitrios Papanastassiou

Seismological Institute, National Observatory of Athens, Greece

and

Shozo Matsumura*

National Research Center for Disaster Prevention, Japan

Abstract

The NRCDP (The National Research Center for Disaster Prevention) operates 67 seismological stations in the Kanto and Tokai areas which are located in central Japan. In the present research, the detection and location capability of this network have been estimated. In addition, the accuracy of the determination of hypocenters and origin time has been investigated, first by using the determination of source parameters as they are recorded in NRCDP's annual bulletins and second by applying the Monte-Carlo method in order to calculate the theoretical errors and to compare these with the actual. For this study, data from the period of 1984 to 1985 have been used.

Contour maps for the locatability of the network and the estimated standard errors (in latitude, longitude, focal depth, origin time) in the earthquake determination have been calculated and plotted.

1. Outline description of NRCDP's observational network

In 1918, the NRCDP started the construction of a high quality network in order to conduct high sensitivity seismic and tilt observations. The network covers the Kanto-Tokai area, which is 400km by 400km. This network has contributed greatly to the national program of Japan for earthquake prediction (Hamada et. al. (1985))

The network consists of 67 seismic stations (Fig. 1). There are 4 kinds of sesmic stations : a) 17 surface stations, b) 2 tunnel stations, c) 45 shallow borehole stations, and

*Second Research Division

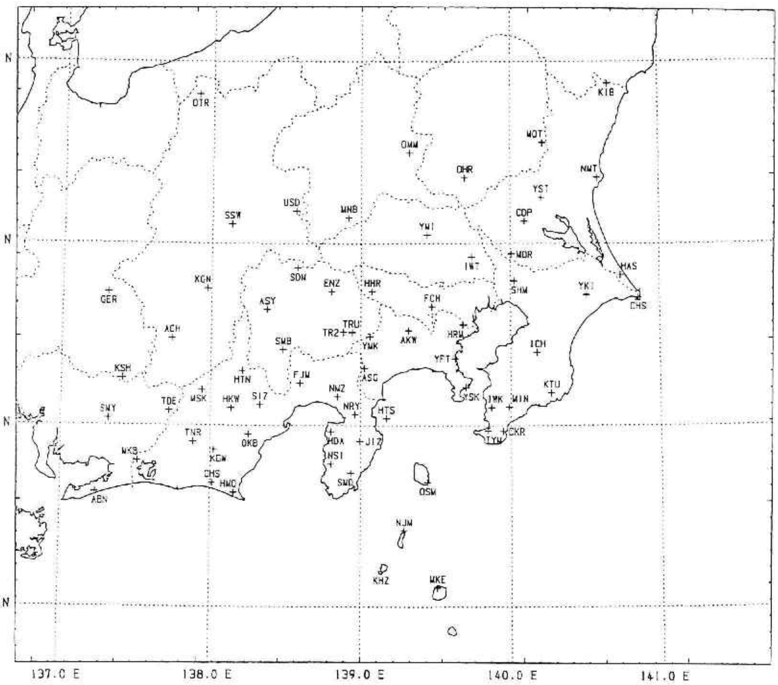

Fig. 1 Kanto-Tokai observational network of the NRCDP as of June 1986.

d) 3 deep borehole stations.

The standard station is a shallow borehole, approximately 100m deep and 4 inches in diameter at the bottom. A vessel containing three components of seismographs and two components of tiltmeters are set at the bottom. The 3 deep borehole stations have depths 3500m, 2710m, 2280m, and reach the basement rock. These stations are located around Tokyo. The construction of these deep boreholes became necessary in order to avoid the high level of artificial noise caused by the city's activity, the influence of the thick soft layers, and to increase the sensitivity of the network at this area. At the bottom, a sensor vessel containing seismometers, accelerometers and tiltmeters is installed (Ohtake and Takahashi (1984)).

Most of the stations have short period three components velocity-type seismometers with a natural frequency of 1.0Hz, a damping constant of h=0.7 and a sensitivity of 2.0 V/kine.

All the seismic signals are telemetered to the NRCDP by using a digital telemetry system, and are recorded on long-term-pen-recorders (continuous recording, only for vertical component) and multichannel-pen-recorders (event triggering method, all the components), and also are processed by an exclusive computer system (Matsumura et. al. (1986)).

There are also stations for other continuous observations such as those for strain, radon emission, acoustic emission, and ground water behaviour.

2. Methodology and analysis

2.1 Detectability-locatability of the network

The knowledge of the detection-location probability is a very important aspect for every seismic network. This term means the ability of one seismic network to detect and locate any earthquake which occurs in the observational area with magnitude larger than a threshold magnitude M_T and coordinates (X, Y, Z).

For this purpose, several methods have been developed to estimate the detection probability function of a seismic network (Deam (1972), Bungum and Husebye (1974), Ringdal (1975), (1976), Seggern and Blandford (1976), Pirhonen et.al. (1976), Shapira et. al. (1979), Lee and Stewart (1981)). Ringdal (1975) has divided these methods into three categories.

1) The indirect estimation method, which is based on seismic noise studies.

2) The recurrence curve estimation method which is based on comparison between the true seismicity and observed detection performance.

3) The direct estimation method which is based on comparison to a reference system.

In this work, we applied the method which was developed by Matsumura (1984) and is based only on the actual data recorded by each seismic station. This method gives the location probability of an observational seismic network by combining the individual detection probability of every single station.

A detailed explanation of this method is given below. First the detection capability of every station is estimated. For this purpose a plot between magnitude and hypocentral distance for the earthquakes which were detected and not-detected at a single station is done (Fig. 2). The separation of detected earthquakes (circles) and not-detected earthquakes (crosses) is clear. However looking at details of the figure, we can see that there are some crosses into the circle 's area and the contrary. This was thought to be mainly due to the effect of the geometrical relation between the hypocenter and the station, and the direction of the focal mechanism. These two regions can be separated by the line derived from the following equations when the maximum amplitude A is fixed :

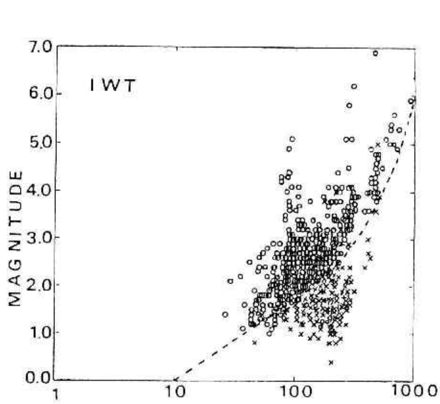

Fig. 2 Magnitude versus hypocentral distance plot of earthquakes which were detected (circles) and not-detected (crosses) at the station IWT.

$$0.85(M-2.04\ \log R)=\log A+2.50 \qquad (R\leq 200\text{km})$$
$$0.85(M-2.04\ \log R-0.0018(R-200))=\log A+2.50 \qquad (R>200\text{km})$$

These equations are given by Watanabe (1971) as the relation among magnitude M, hypocentral distance R in km, and maximum amplitude A in kine for regional earthquakes.

The line passes through the point of 50% probability. We can transform these axes systems into others by reducing the magnitude axis. Setting the reduced magnitude M' $=M-2.04\ \log R$ for R less than 200km, we can define the detection probability of earthquakes at a single station as a function of M' as follows :

Detection probability
= (Number of detected earthquakes) / (Total number of detected and not-detected earthquakes)

Figure 3 shows plots of these values at the station IWT. Approximating these plots by a cumulated normal distribution function Φ, we can express the detection probability of the i-th station in an analytical form as :

$$p_i(M, R)=\Phi\ [(M'-\mu_i)/\sigma_i]$$

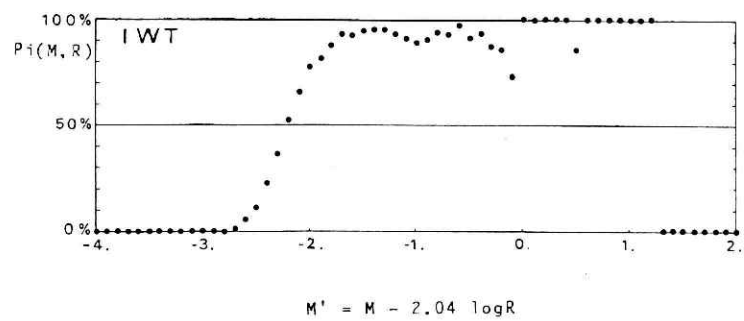

Fig. 3 Detection probability as a function of the reduced magnitude M'.

The mean value μ_i is directly related with the sensitivity of the station. The smaller the value of μ_i, the more sensitive is the station. The standard deviation σ_i as it is well known, represents the scattering of the points around the mean value. Table 1 gives the values of μ_i and σ_i for all the stations. Figure 4 shows the geographical distribution of the μ_i values. The high sensitivity of the deep borehole stations in comparison with the neighbouring stations is obvious.

In order to calculate the locatable probability, we divide the observational area into

Table 1 Locations of the stations and μ, σ values.

STATION	LAT.(°N)	LON.(°E)	HEIGHT(Km)	μ	σ
ABN	34.629	137.234	0.040	-2.34	0.28
ACH	35.475	137.738	0.762	-1.76	0.21
AKW	35.520	139.318	-0.010	-1.59	0.24
ASG	35.314	139.028	0.386	-1.90	0.26
ASY	35.635	138.373	0.800	-1.58	0.26
CDP	36.122	140.093	-0.620	-1.38	0.18
CHS	35.702	140.855	-0.042	-1.13	0.28
ENZ	35.736	138.805	0.807	-1.70	0.26
FCH	35.651	139.474	-2.707	-1.92	0.29
FJM	35.233	138.597	-0.059	-1.28	0.19
GER	35.727	137.305	0.620	-2.56	0.36
HAS	35.826	140.736	-0.784	-1.26	0.26
HCJ	33.073	139.843	0.036	-1.06	0.45
HOA	34.965	138.805	-0.046	-1.46	0.32
HHR	35.735	139.076	0.595	-1.90	0.49
HKW	35.093	138.138	0.343	-2.13	0.44
HMO	34.631	138.159	-0.061	-1.22	0.35
HRM	35.551	139.679	-0.536	-0.84	0.19
HTN	35.300	138.211	0.855	-1.94	0.39
HTS	35.039	139.172	-0.084	-1.30	0.32
ICH	35.401	140.177	-0.146	-0.87	0.28
IWK	35.098	139.871	0.010	-1.42	0.36
IWT	35.926	139.738	-3.501	-2.21	0.22
JIZ	34.913	138.997	0.263	-1.92	0.34
KGN	35.752	137.972	0.629	-1.94	0.28
KGW	34.863	138.022	0.069	-2.08	0.49
KHZ	34.196	139.139	0.053	-0.62	0.42
KIB	36.878	140.658	0.298	-2.36	0.29
KSH	35.258	137.409	0.343	-2.14	0.28
KTU	35.177	140.269	-0.012	-1.16	0.28
MIN	35.102	139.991	0.112	-1.43	0.39
MKB	34.802	137.514	-0.038	-2.00	0.28
MKE	34.106	139.510	0.164	-1.08	0.38
MNB	36.141	138.917	0.895	-1.78	0.26
MOR	35.943	140.004	0.001	-0.50	0.43
MOT	36.554	140.217	0.140	-2.26	0.20
MSK	35.193	137.939	0.754	-2.26	0.56
NJM	34.420	139.288	0.050	-0.84	0.35
NMT	36.362	140.584	-0.075	-1.00	0.20
NMZ	35.158	138.846	0.114	-1.30	0.27
NRY	35.060	138.963	-0.091	-1.62	0.30
NSI	34.787	138.804	-0.422	-2.10	0.24
OHR	36.360	139.692	0.244	-2.38	0.19
OHS	34.683	138.015	-0.067	-1.04	0.27
OKB	34.950	138.254	-0.032	-1.63	0.32
OMM	36.497	139.321	0.463	-2.15	0.32
OSM	34.688	139.443	-0.044	-0.94	0.26
OTR	36.818	137.903	0.575	-1.45	0.26
SOM	35.864	138.577	1.270	-2.22	0.28
SHM	35.793	140.024	-2.277	-2.34	0.28
SIZ	35.112	138.330	0.076	-1.79	0.38
SMB	35.416	138.483	0.202	-2.04	0.24
SMO	34.738	138.934	-0.013	-2.00	0.27
SMY	35.037	137.316	0.303	-2.41	0.21
SSW	36.106	138.133	0.987	-1.86	0.33
TNR	34.908	137.885	0.066	-2.03	0.41
TOE	35.078	137.724	0.255	-2.48	0.27
TRU	35.511	138.944	0.565	-1.84	0.32
TR2	35.512	138.887	0.151	-1.94	0.31
TYM	34.971	139.848	0.030	-1.36	0.34
USD	36.181	138.564	0.969	-2.02	0.33
YFT	35.368	139.629	-0.026	-1.18	0.34
YKI	35.719	140.509	-0.142	-1.00	0.48
YMI	36.048	139.440	-0.052	-1.63	0.35
YMK	35.487	139.063	0.564	-2.22	0.33
YSK	35.208	139.700	-0.189	-1.30	0.29
YST	36.253	140.206	-0.071	-2.20	0.21

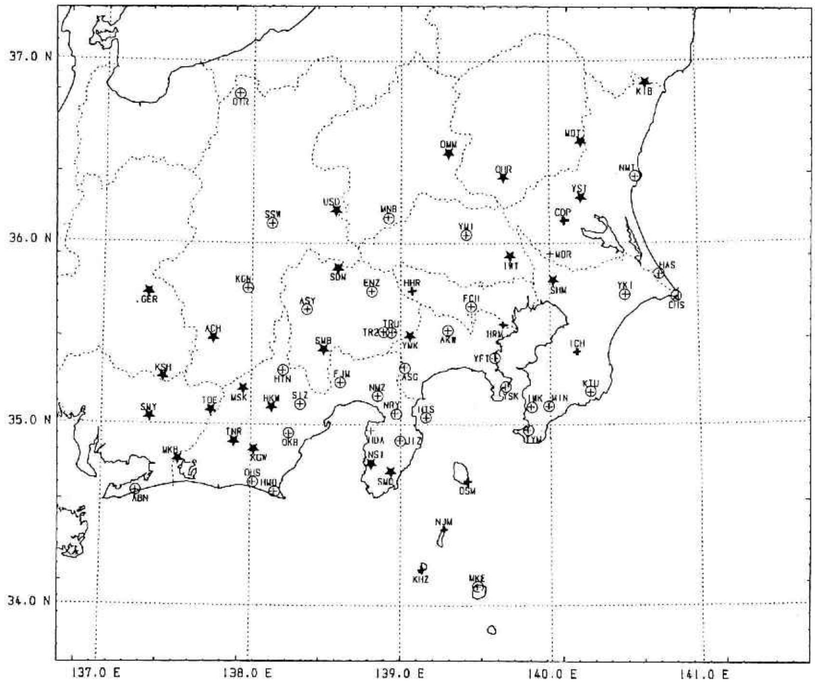

Fig. 4 Geographical distribution of μ values. The marks have the following meaning : ★ ≤ -2.0 ; $-2.0 < \oplus \leq -1.0$; $-1.0 < +$

small squares, 10km by 10km. In every square, we assume that a single earthquake occurs with fixed magnitude M_T at different depths. Then we can calculate the locatable probability P of the network under the condition that the earthquake must be detected at more than 2 stations. So,

$$P(M_T, X) = 1.0 - (P_0 + P_1 + P_2)$$

Where X represents the position of the earthquake, and P_n means the probability that the earthquake could be detected at only n stations as follows :

$$P_0 = (1 - p_1)(1 - p_2) \ldots . (1 - p_N)$$

$$P_1 = p_1(1 - p_2)(1 - p_3) .. (1 - p_N) + .. + p_N(1 - p_1)(1 - p_2) .. (1 - p_{N-1})$$

$$P_2 = p_1 p_2 (1 - p_3) \ldots\ldots . (1 - p_N) + .. + p_{N-1} p_N (1 - p_1) \ldots (1 - p_{N-2})$$

Where N is the total number of the stations of the network.

The results are shown as three dimensional maps in Fig. 5(a), (b), (c), and Fig. 6 where, inside the volume shown with contours, every earthquake with a magnitude greater than the fixed threshold magnitude M_t can be detected and located with a probability larger than 95%.

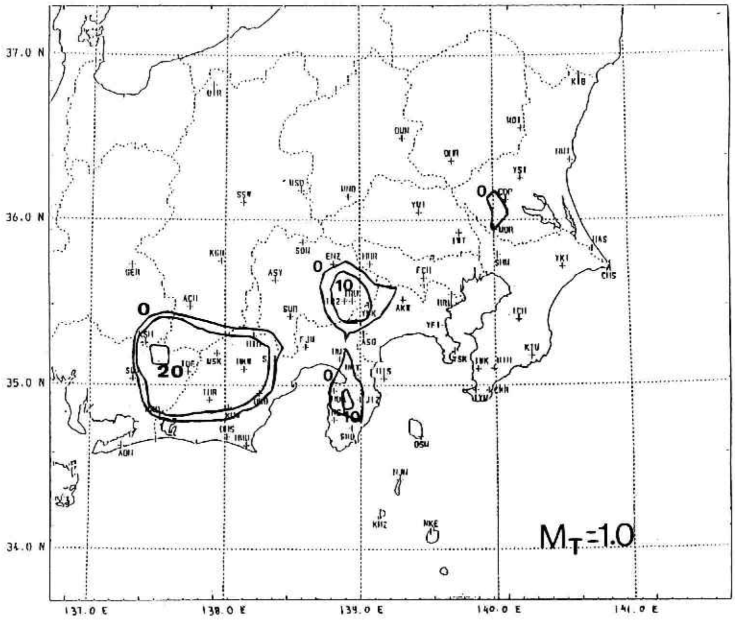

Fig. 5 The contours show the three-dimensional feature of the region, inside which earthquakes greater than the threshold magnitude M_T are detected and located with a probability larger than 95%. The numbers of the contours indicate depths in the unit of km.
(a) $M_T=1.0$

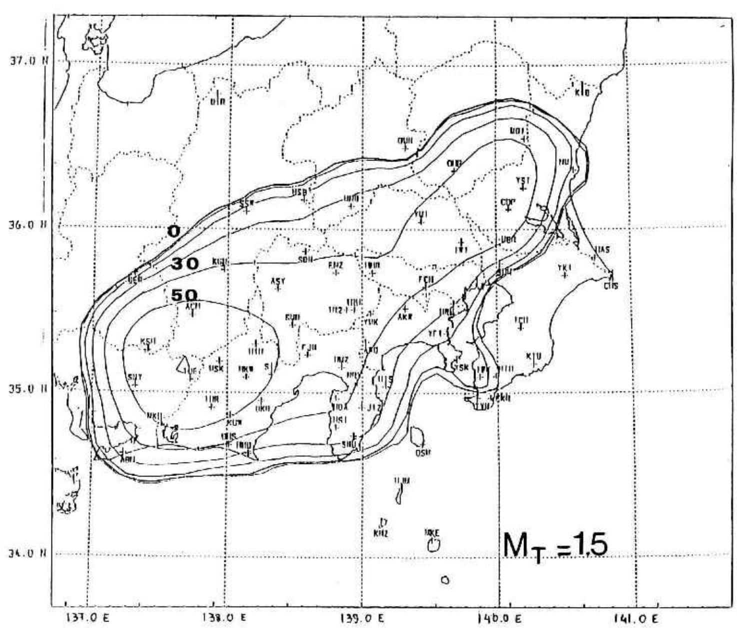

(b) $M_T=1.5$

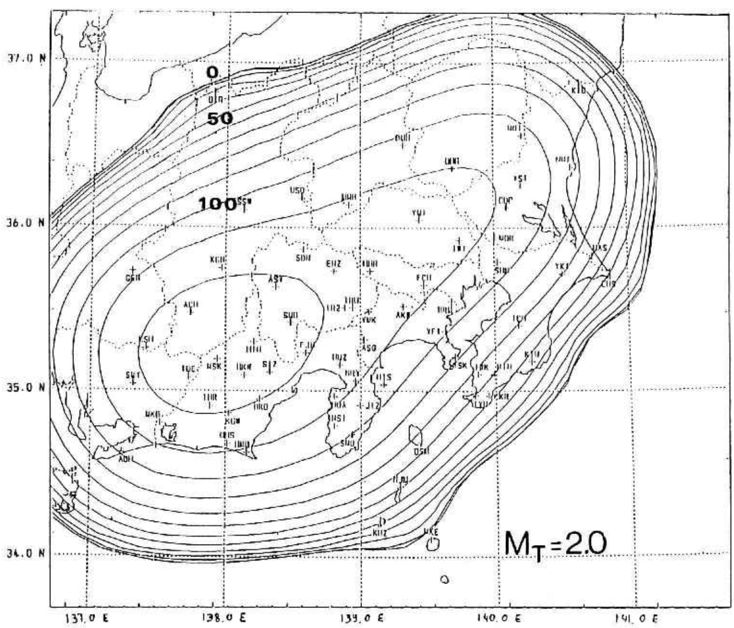

(c) $M_T = 2.0$

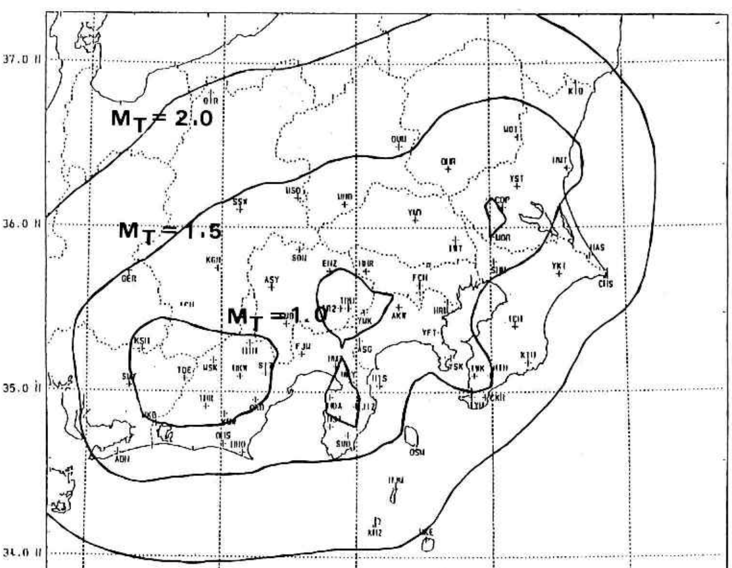

Fig. 6 The contours show 95% locatable regions on the surface for various threshold magnitude M_T.

2.2 Performance of the routine triggering system for the three deep borehole stations

Besides the routine triggering system, there is a special triggering system for seismic observations around Tokyo which utilizes deep borehole stations. In order to compare the detection capability of the three deep borehole stations in the routine triggering system with those in the special triggering system, we carried out a separate examination. We checked the detectability of these stations for the period May-August 1983 because, during this period, the three stations performed at their best. The results for the μ and σ values are listed in Table 2. These results confirm that the routine triggering system carried out by the exclusive computer system of the NRCDP helps the three borehole stations, keeping their sensitivity at high levels.

Table 2 Comparion of capability parameters for the three deep borehole stations between in the routine triggering system and in the special triggering system.

	DATA 1984−85			DATA 1983		
	ROUTINE triggering system			SPECIAL triggering system		
	FCH	IWT	SHM	FCH	IWT	SHM
μ	−1.92	−2.21	−2.34	−1.90	−2.32	−2.24
σ	0.29	0.22	0.28	0.44	0.28	0.32

2.3 Optimum position for the construction of a new deep borehole station

The NRCDP wants to improve the detectability-locatability of the network, especially in the vicinity area of Tokyo by constructing, in the future, the fourth deep borehole.

Consequently, we tried to find out the 'optimum' place for this new station. Thus far many papers have been published on the optimum distribution of seismic stations. These papers have treated this problem using statistical methods in the hope of minimizing the errors which come in the hypocentral determination. Sato and Skoko (1965) used a Monte-Carlo method to distribute random observation points so that the errors in the determination of the coordinates of the focus and the origin time of the earthquake would be very small. Kijko (1977) solved this problem with a method which minimized the random errors (errors which depend upon the accuracy of the readings of seismic wave arrivals and the geometry between the hypocenter and seismic station). In our work we did not follow any of these methods. Instead, we solve the problem using a rather practical method based on the already obtained results of the sensitivity of the stations. We supposed reasonable values for the depth, the mean value μ, and the standard deviation σ of the new station. Dividing the observational area in squares of 20km by 20 km, and locating the new station at every square, we had measured the locatable volume revised. Comparing these results with the existing ones, we could draw maps Fig. 7(a) and (b) showing the increase of the locatable volume. Then the 'optimum' position is those places where this value becomes maximum. Looking over these figures, we selected a candidate for the new station at the tip of the Boso peninsula. Improvements of the locatable areas are clearly shown in Fig. 8(a), (b), and (c) which are given in the same manner as Fig. 5 and 6.

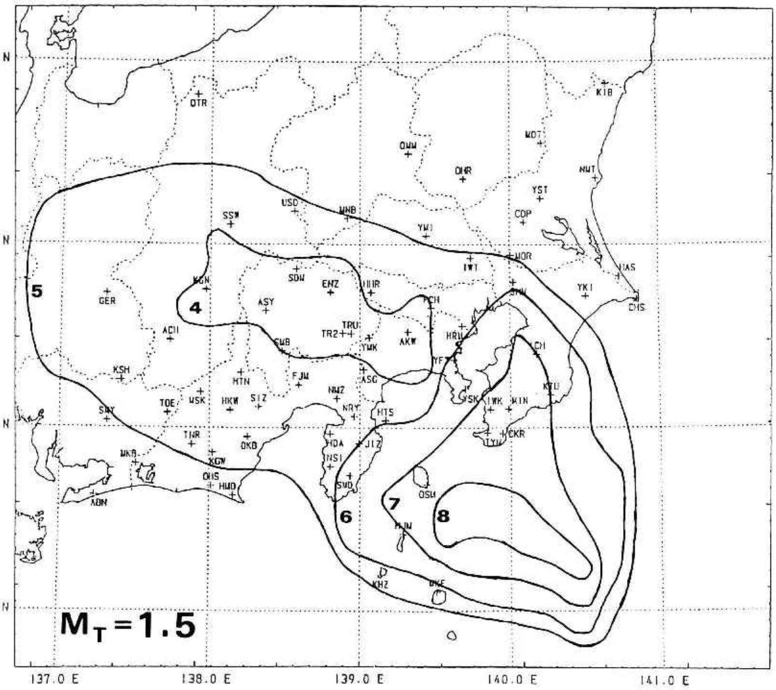

Fig. 7 Increasing (per cent) of the locatable volume when the fourth new deep borehole station is added to the network.
(a) $M_T = 1.5$

2.4 Accuracy of the determination of earthquake source parameters

a) Actual data

In the annual bulletins of the NRCDP, the standard deviations for the hypocenter and origin time determinations have been recorded. We used these values in order to examine the actual errors in the determination of earthquake parameters. We did not use the solutions with standard errors larger than 10km for horizontal coordinates, 20km for focal depth, and 2 sec for the origin time, because determinations with values larger than the above were out of 95% confidence limits of the normal distribution which the standard deviations follow.

We separated the observational area into two regions, eastern and western, with a boundary of 139°E, and we examined the focal depth distribution of earthquakes belonging to each region (Fig. 9(a), (b)). In the western region, the majority of the earthquakes have depths less than 25km with a peak at the depth of 10km. In the eastern

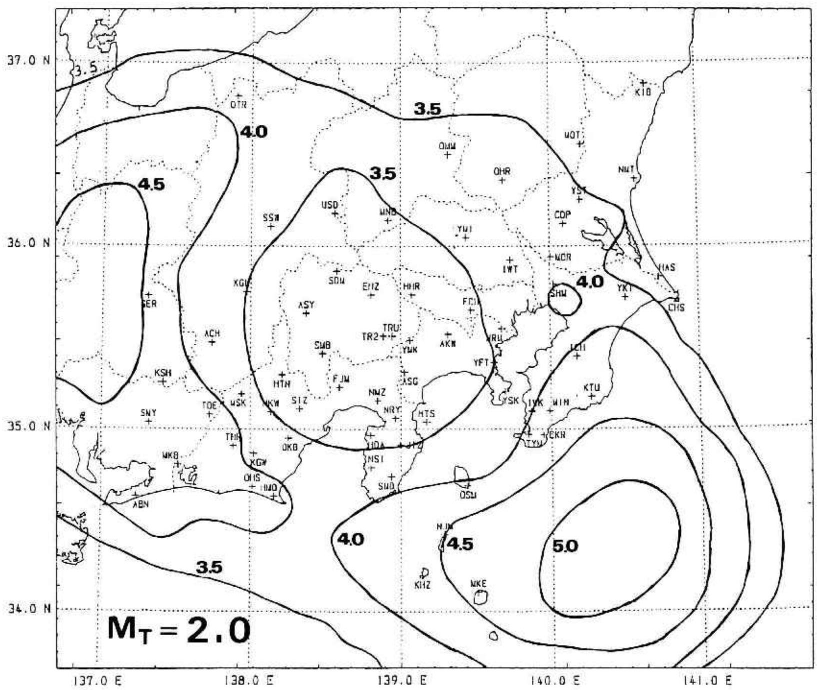

(b) $M_T=2.0$

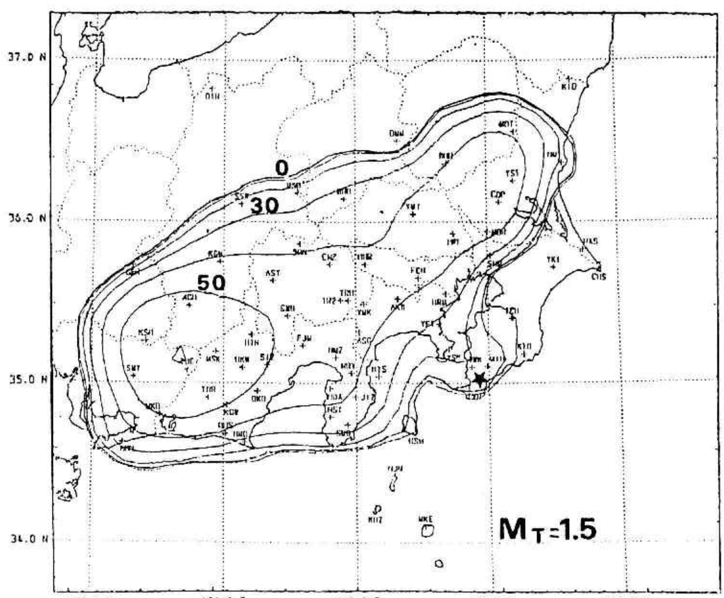

Fig. 8 The detection-location capability of the network revised with an assumed new deep borehole station. The star shows the position of the new station. Compared with Fig. 5(b), (c), and Fig.6, improvements are clearly found around the Boso peninsula.

(a) $M_T=1.5$

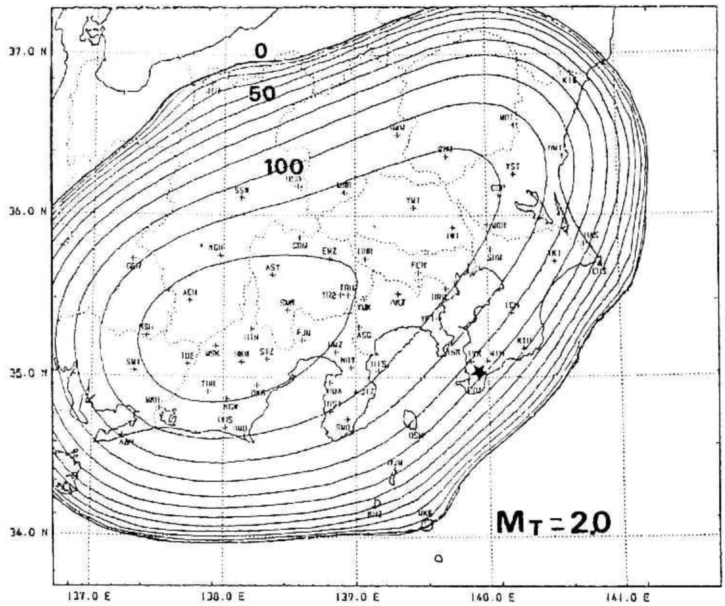

(b) $M_T = 2.0$

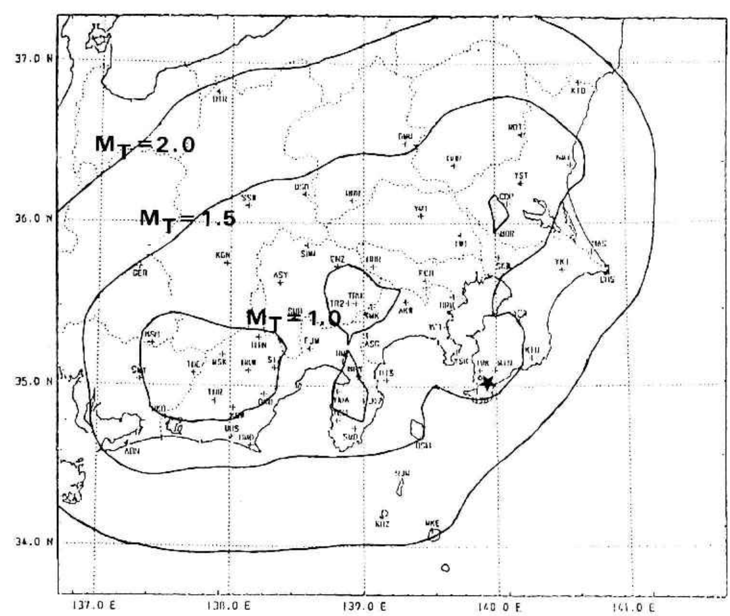

(c) Surface contours for $M_T = 1.0$, 1.5 and 2.0

region, the distribution is quite different. There is a maximum peak in the depth range of 10-20km, and two smaller peaks in the ranges of 40km-45km and 60-70km. For these reasons, we divided the whole area along the depth axis, and for further investigation, into three layers as follows : a) 0-24km, b) 25-100km, and c) 101-200km. At every layer, we divided the area into small squares of 10km, by 10km and then calculated and plotted the mean value of the standard deviations, with a restriction that in every cube at least 5 earthquakes occurred. The results are shown in Fig. 10, 11, and 12.

b) Theoretical errors

There are many factors influencing accuracy of determination of earthquake source parameters. These include such factors as the reading of the arrival time of seismic wave phases, the travel time tables assumed which are used for the determination, and the geographical relation between epicenters and the distribution of the stations. As it is well known, the epicenter can be best located when the seismic stations are regularly distributed around it. In addition, the focal depth can be accurately obtained when the epicentral distance from at least one station is not greater than the depth. So, it is obvious that the distribution of the stations plays a very significant role in the measure of the errors which are expected in the determination of the parameters of the focus.

We followed the Monte-Carlo method which is described by Skoko et.al. (1966). We expanded this method so that we can calculate the errors in both the horizontal directions and also in the depth. We assume, for the case of simplicity, that the observational accuracy is the same for all the stations, and the error follows the normal distribution with a mean value of 0 and a deviation of ε^2. The equation which connects the error of

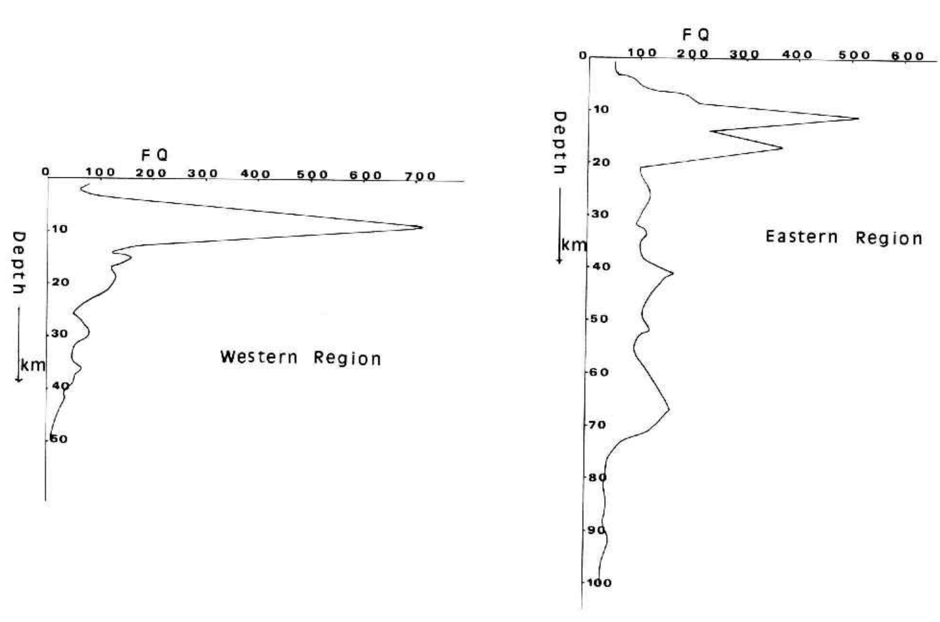

Fig. 9 Focal depth distribution of earthquakes.
(a) Eastern region, (b) Western region

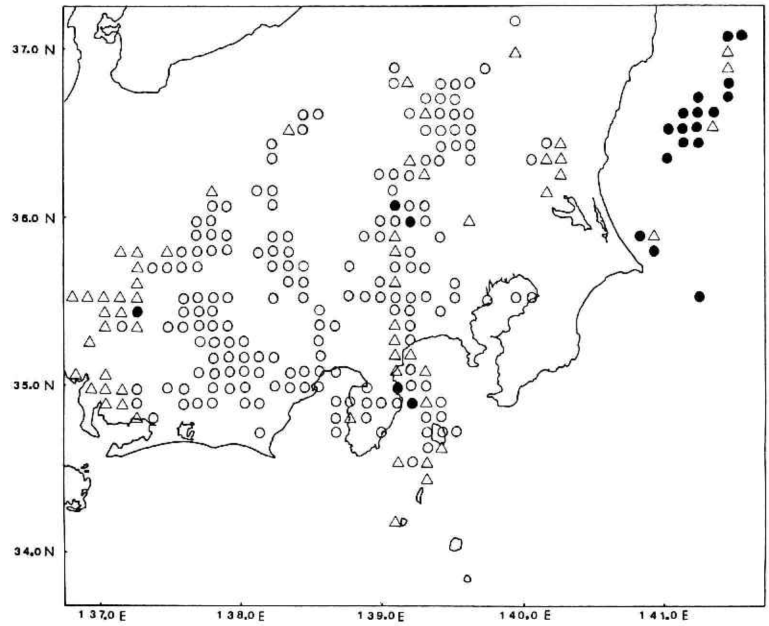

Fig. 10 Actual errors for earthquake source parameters with focal depths 0-24km.
(a) X direction : ○≦1km, 1km<△≦2km,2km<●

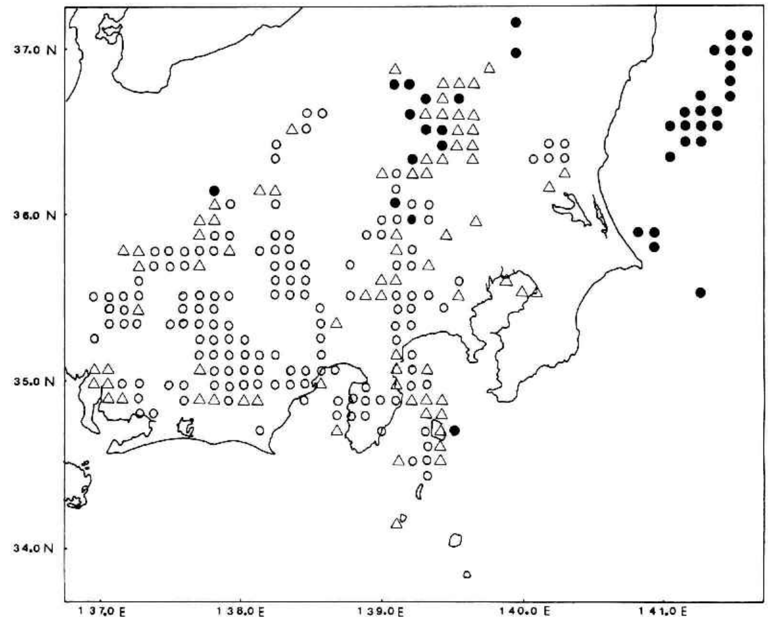

(b) Y direction : ○≦1km,1km<△≦2km,2km<●

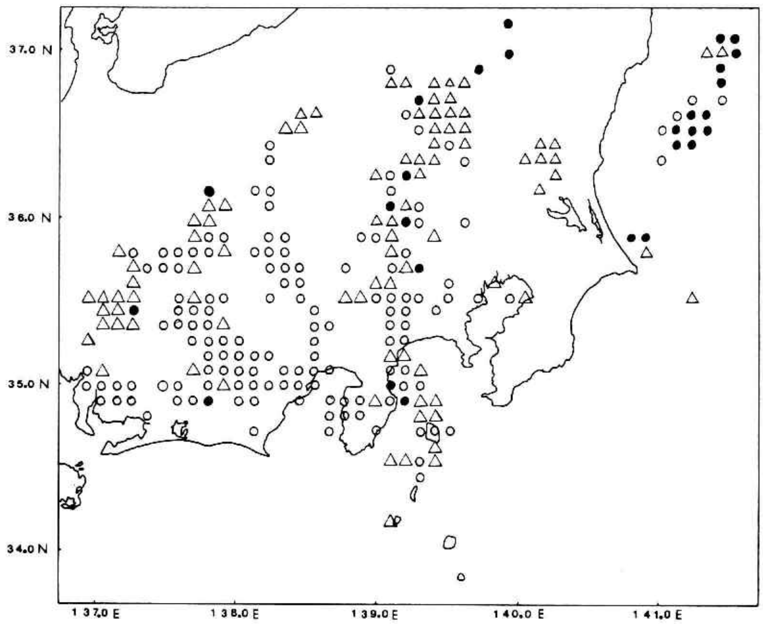

(c) Focal depth : ○≤2km, 2km<△≤4km, 4km<●

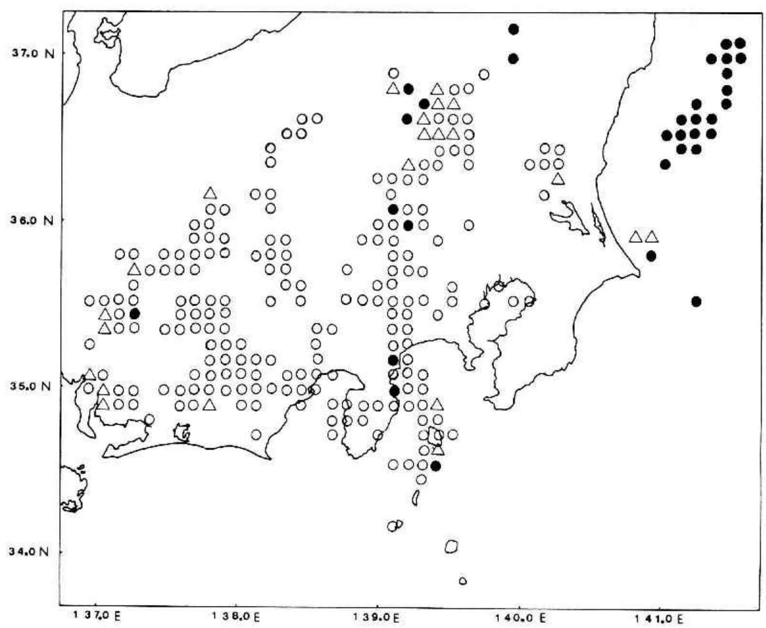

(d) Origin time : ○≤0.2sec, 0.2sec<△≤0.3sec, 0.3sec<●

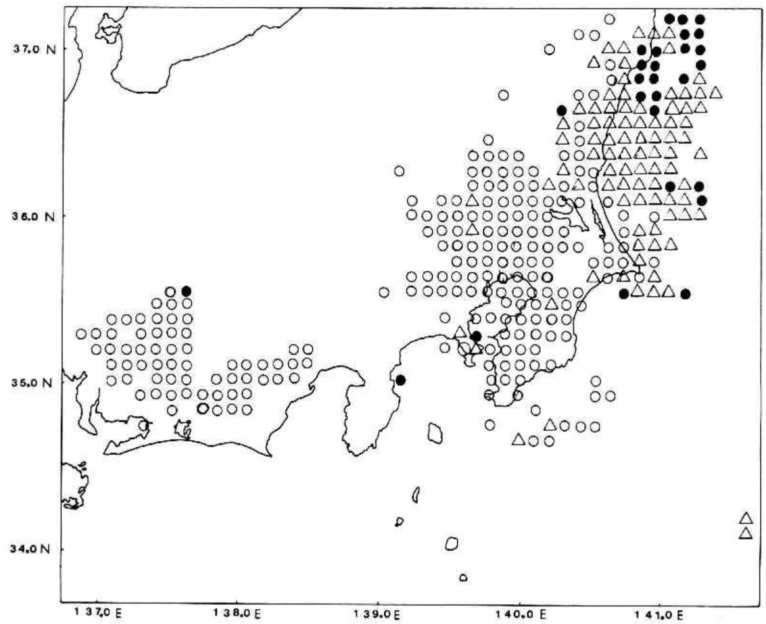

Fig. 11 Actual errors for earthquake source parameters with focal depths 25-100km.
(a) X direction :○≤2km, 2km<△≤3km,3km<●

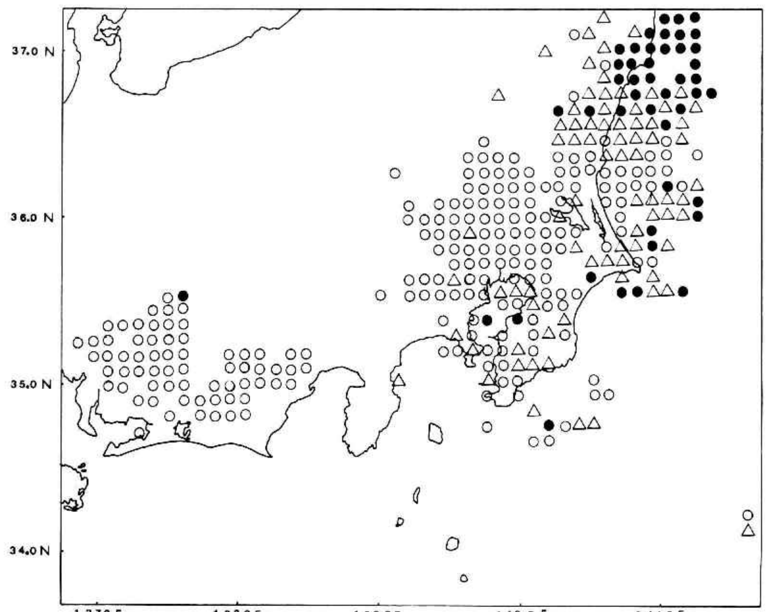

(b) Y direction : ○≤2km,2km<△≤3km,3km<●

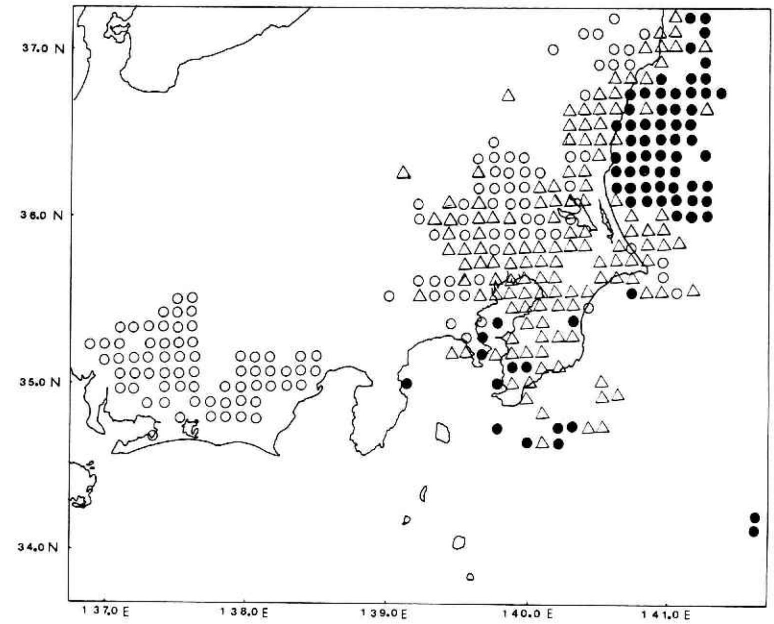

(c) Focal depth : ○≦2km,2km<△≦4km,4km<●

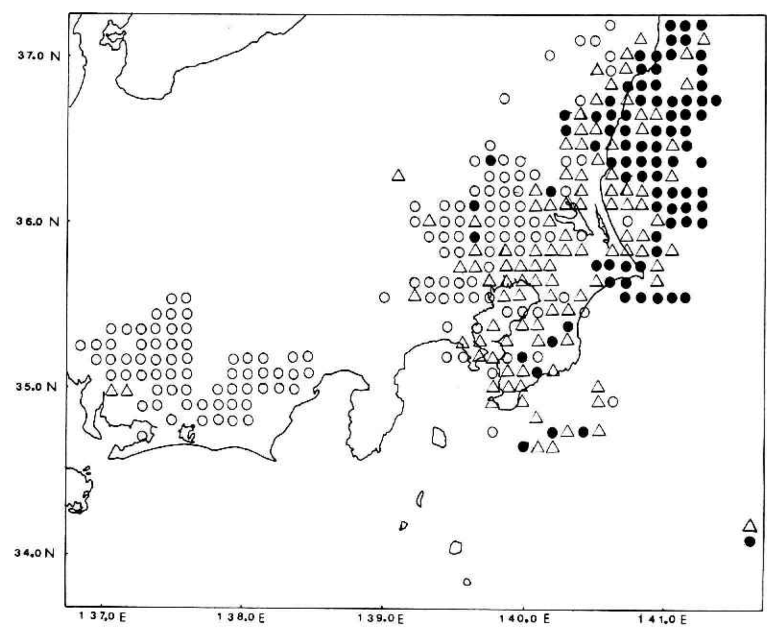

(d) Origin time : ○≦0.2sec, 0.2sec<△≦0.3sec, 0.3sec<●

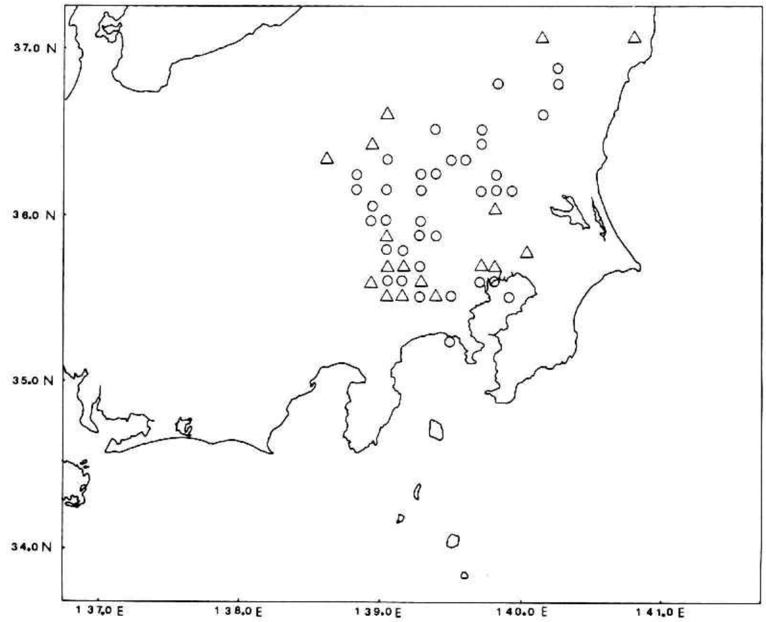

Fig. 12 Actual errors for earthquake source parameters with focal depths 101–200km.
(a) X direction : ○≦2km, 2km<△

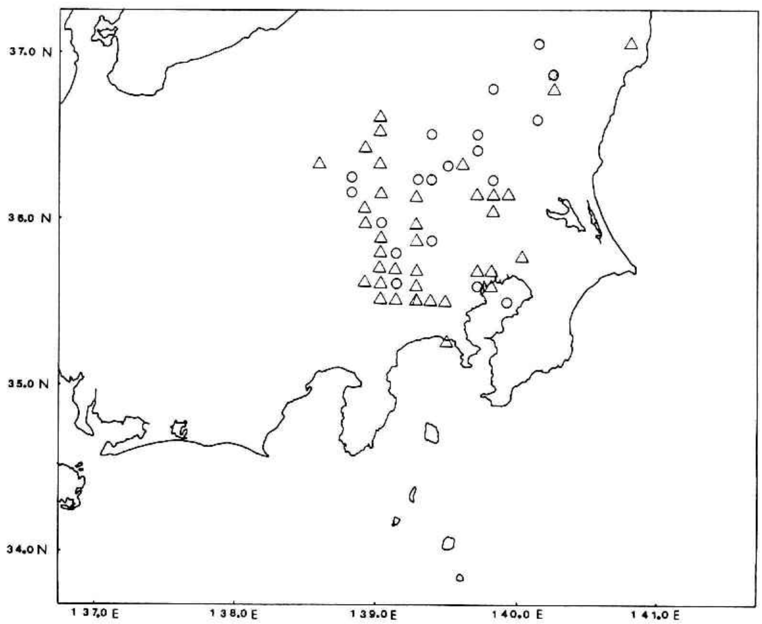

(b) Y direction : ○<2km, 2km<△

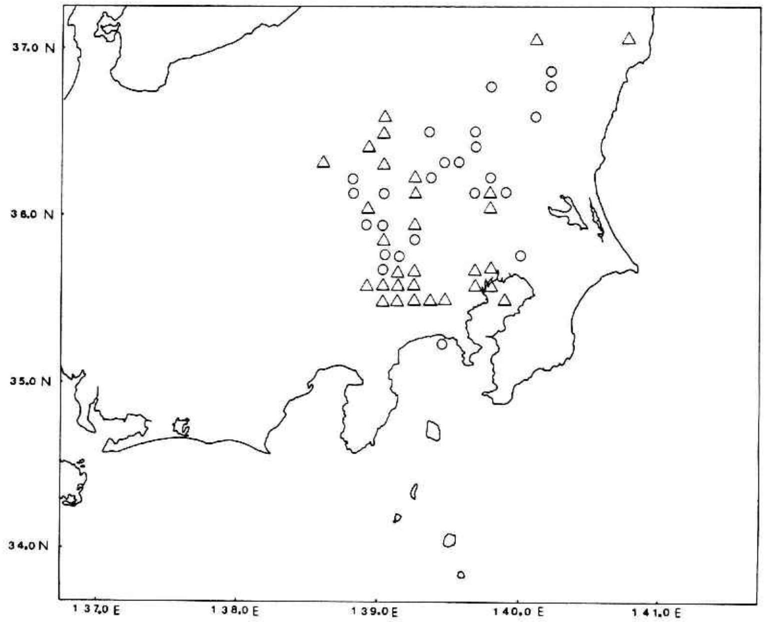

(c) Focal depth : ○≤2km, 2km<△

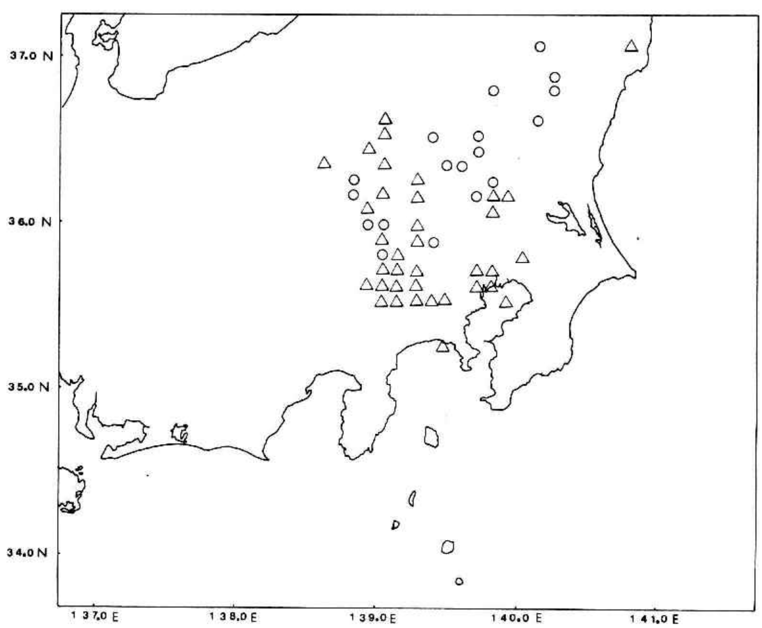

(d) Origin time : ○≤0.2sec, 0.2sec<△

calculated parameters (X, Y, Z direction and origin time), the location of the stations and the travel time of the seismic wave is as follows :

$$\left(\frac{\partial f}{\partial \Delta}\right)_k dx \sin\theta_k + \left(\frac{\partial f}{\partial \Delta}\right)_k dy \cos\theta_k + \left(\frac{\partial f}{\partial \Delta}\right)_k dz + dt = \varepsilon_k$$

where

$f(\Delta, Z)$	: travel time
θ_k	: azimuth at the epicenter measured clockwise from the north to the station k
dx, dy, dz	: distance between the true and calculated hypocenter in X, Y, and Z direction, respectively
dt	: error of the origin time
k	: index number of the station
ε_k	: observational error of the arrival time at each station
Δ	: epicentral distance

The true epicenter is assumed to be at the origin of our coordinate system. Figure 13 shows the configuration of the problem. In order to solve this problem, it is necessary to know the derivatives of the travel time. Ukawa et.al (1984) presented a model travel time and a subroutine program to calculate its derivatives using an assumed horizontally uniform velocity structure. On this basis, we solved the above equation with four unknown parameters dx, dy, dz, and dt. First, we located the hypocenters at intervals of 10km both in latitude and longitude, with three cases of depths 10km, 50km, and 100km. Then, we computed the coefficients for the left-hand side of the equation. The right-hand side terms of the equation were determined by giving values out of series of normally distributed random numbers with a mean value of 0 sec and a standard deviation of 0.3 sec. For each hypocenter, 67 equations are given as the number of the stations. By using the least square method, the unknown parameters can be obtained. This procedure was repeated 100 times and the standard deviations were calculated as the final solution for the four unknown parameters. The results were smoothed, and the general trend of the errors are shown as the functions of the hypocenter locations in Fig. 14 to 16.

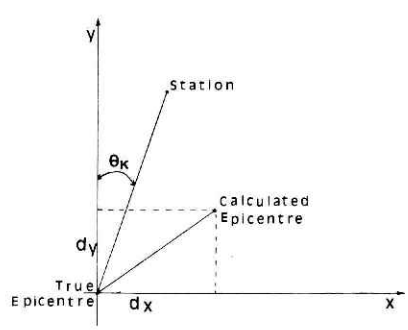

Fig. 13 Relationship between station , true epicenter, and assumed epicenter for the calculation of the theoretical errors.

3. Discussion and conclusions

From Fig. 4, we can see that the distribution of the stations is not homogeneous, based on their sensitivity (μ value). The western stations are more sensitive than the eastern ones. The main factor for this is that the western area is mountainous with low background noises due to the presence of the hard bed-rocks. On the contrary, the eastern region is industrial with thick soft layers of sediments and high artificial noises. These reasons affect the detection capability of the whole network. From Fig. 5(a), (b), and (c), we can conclude that shallow earthquakes (depth$\leq$50km) with a magnitude greater than 2.0 could certainly be detected within the observational area. For earthquakes with smaller magnitudes, the network has a gap in the locatable region at the east side of the Boso Peninsula.

During the trial to find out the 'optimum' position for the construction of the new deep borehole station, we took into consideration the fact that one of the main purpose of the NRCDP is the prediction of the coming Tokai earthquake. After a careful examination, we selected the area of the Boso peninsula from all possible positions. In this area, the sensitivity of the network is not so high and, in addition, the area itself is located above the subducting Philippine sea plate. In the end, we located the new station at the southern part of the Boso peninsula as the optimum position. The improvement of the locatability of the network from adding this new station is clear, especially in the Boso area as shown in Fig. 8(a), (b), and (c).

Though it is difficult to draw a smooth contour for determining error distributions obtained from the actual data due to the non-uniform concentration of earthquakes, we can get some trends from Fig. 10, 11, and 12. For the shallow earthquakes with depths of 0-24km, the results are shown in Fig. 10(a), (b), (c), and (d). Inside the network area, the standard deviations are less than 1.0km for the horizontal positions, 0.6-4.0km for the focal depth and less than 0.3 sec for the origin time. On the other hand, outside the network, these deviations show greater values in general. For the middle depth range of 25-100km shown in Fig. 11 (a), (b), (c), and (d), the majority of the earthquakes are concentrated in the eastern part, and the standard deviations are 1.0-3.0km for the horizontal positions, 1.0-5.0km for the focal depth, and less than 0.4 sec for the origin time. These values are larger than those for shallower earthquakes, as expected. For the deep depth range of 101-200km shown in Fig. 12(a), (b), (c), and (d), the data are too few to present some significant conclusions.

Figures 14 to 16 show the theoretical errors for the hypocenter and the origin time estimation as functions of hypocentral location with various depths. From these diagrams, we can get some ideas on the accuracy of the determination of the earthquake parameters.

Comparing these results with the actual standard deviation, we can see a general similarity between them, despite some local anomalies found in the actual data, for example, in the vicinity of the Izu peninsula. The latter should be due to some inhomogeneities of the velocity structure in the real situation.

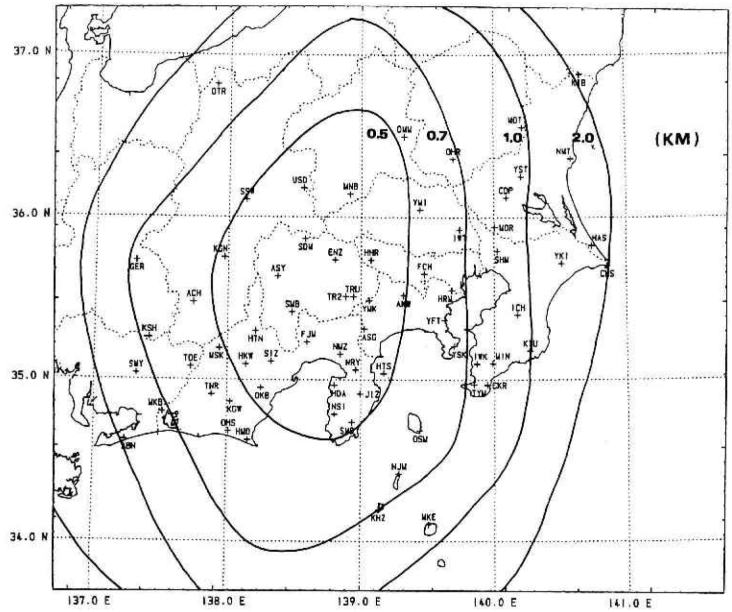

Fig. 14 Theoretical errors for earthquake source parameters with a focal depth 10km.
(a) X direction (km)

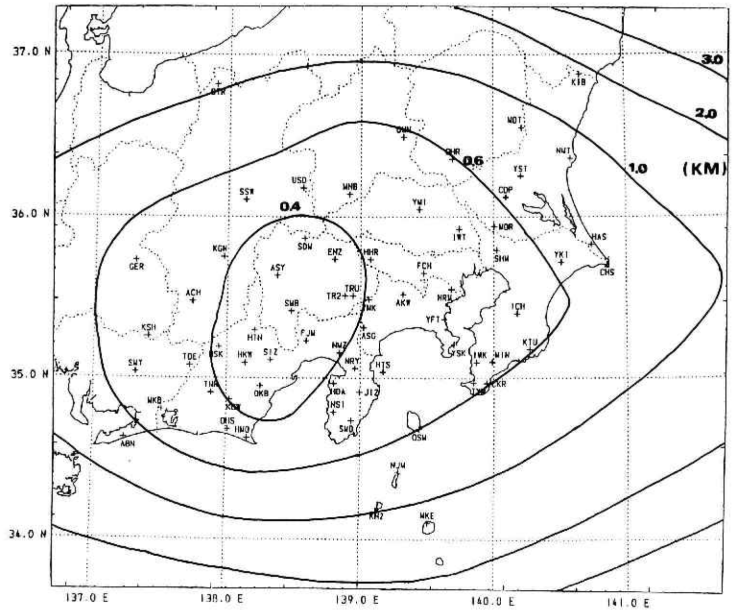

(b) Y direction (km)

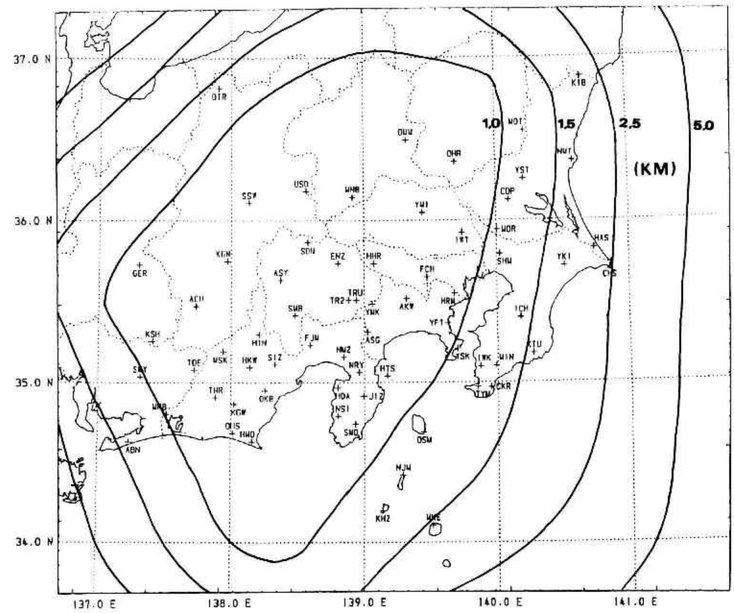

(c) Focal depth (km)

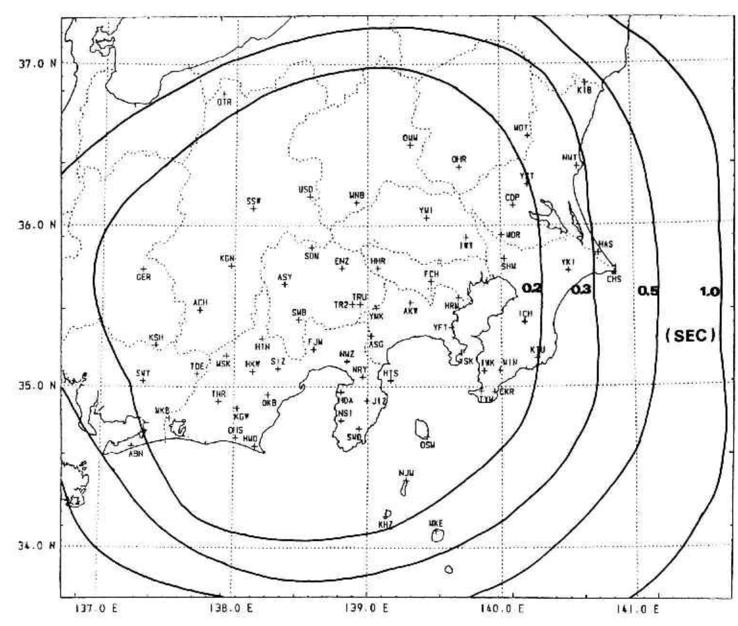

(d) Origin time (sec)

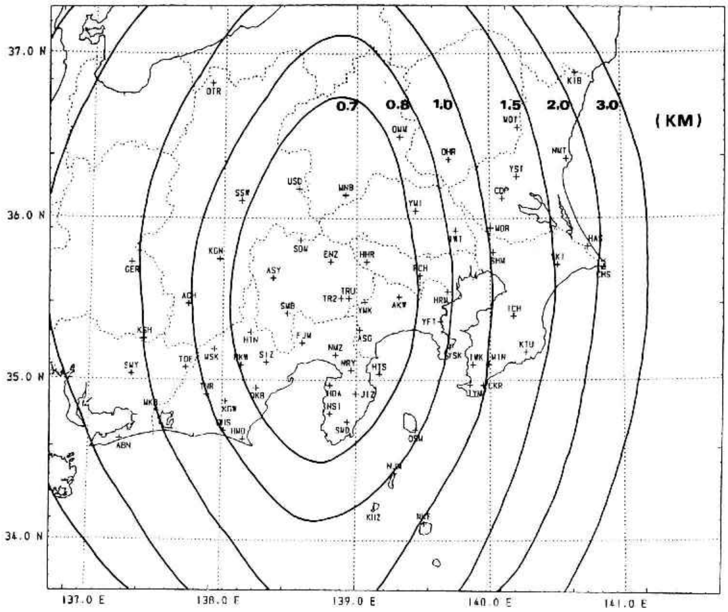

Fig. 15 Theoretical errors for earthquake source parameters with a focal depth 50km.
(a) X direction (km)

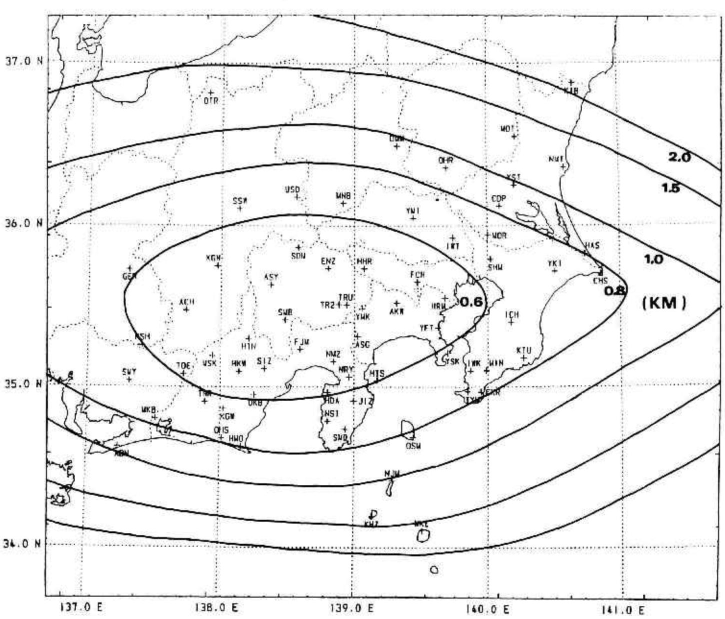

(b) Y direction (km)

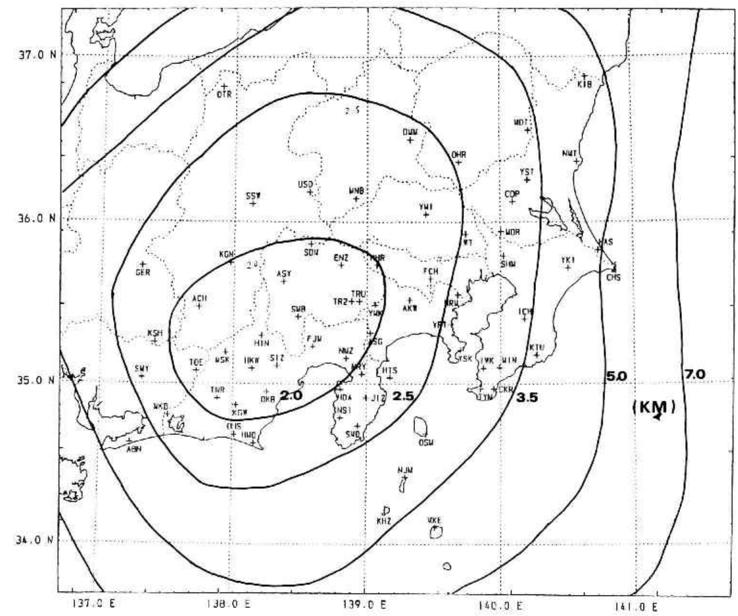

(c) Focal depth(km)

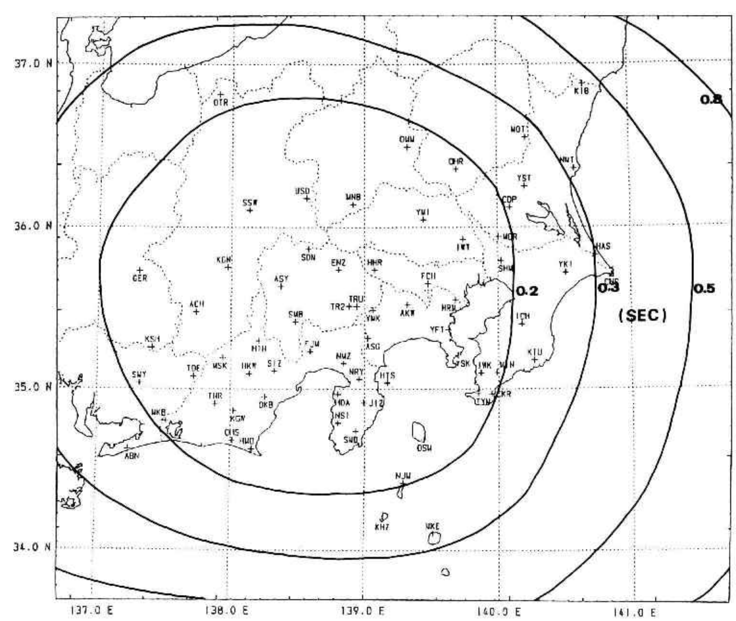

(d) Origin time (sec)

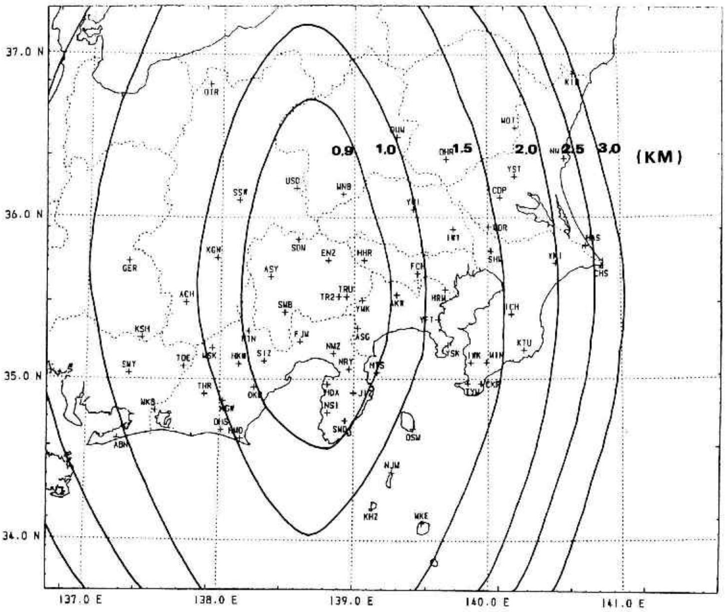

Fig. 16 Theoretical errors for earthquake source parameters with a focal depth 100km.
(a) X direction (km)

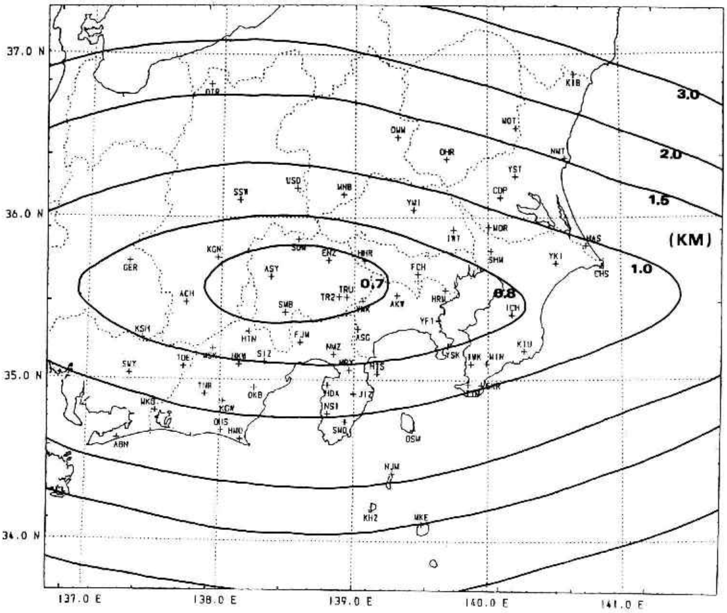

(b) Y direction (km)

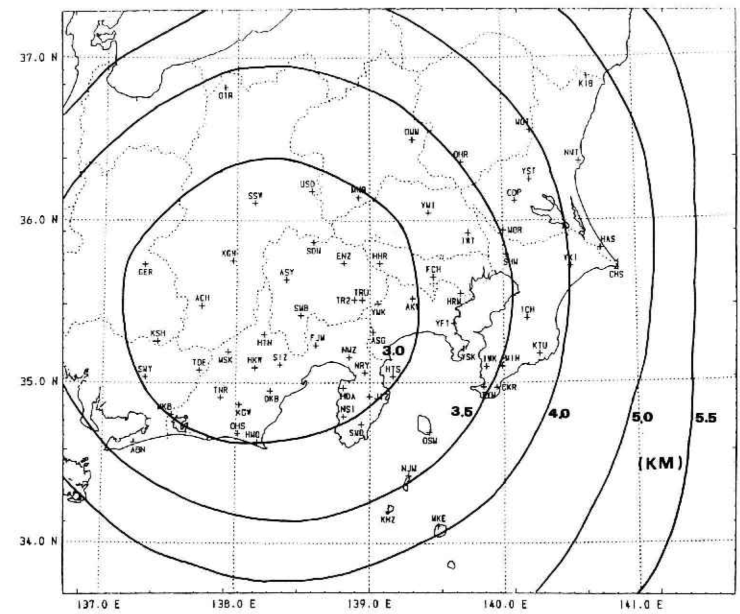

(c) Focal depth (km)

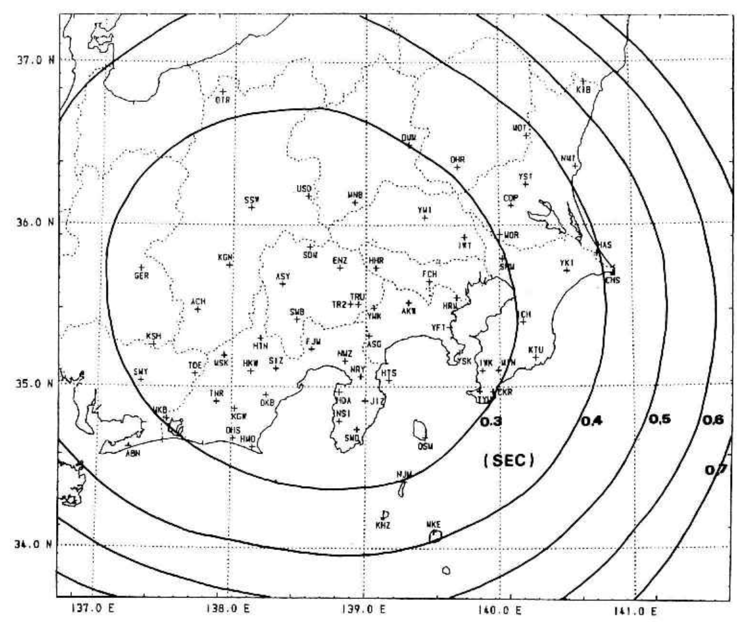

(d) Origin time (sec)

Acknowledgements

The authors wish to thank H. Takahashi, the director general of the NRCDP and to S. Hattori, the director of the International Institute of Seismology and Earthquake Engineering for all the assistance offered by them and the kind permission to publish this study. In addition, we express our sincere thanks to K. Hamada, M. Ohtake, and M. Ukawa for their useful comments and suggestions, and to K. Obara and M. Takahashi for offering invaluable data.

References

1) Bungum, H. and S. Husebye (1974) : Analysis of the operational capabilities for detection and location of seismic events at NORSAR. Bull. Seism. Soc. Am., **64**, 637-656.
2) Dean, W. (1972) : Detection threshold of the LASA/SAAC system. Geophys. J. Roy. Astr. Soc., **31**, 271-278.
3) Hamada, K., M. Ohtake, Y. Okada, S. Matsumura and H. Sato (1985) : A high quality digital network for microearthquakes and ground tilt observations in the Kanto-Tokai area, Japan. Earthq. Predict. Res., **3**, 447-469.
4) Kijko, A. (1977) : An algorithm for the optimum distribution of a regional seismic network-I. Pageoph., **115**, 999-1009.
5) Kijko, A. (1977) : An algorithm for the optimum distribution of a regional seismic network-II. An analysis of the accuracy of location of local earthquakes depending on the number of seismic stations. Pageoph., **115**, 1011-1021.
6) Lee, W. H. K. and S. Stewart (1981) : Principles and applications of microearthquake networks. Academic press, 293p.
7) Matsumura, S. (1984) : Evalution of detection capability of microearthquakes for an observational network. ZISIN **2**, **37**, 475-489.
8) Matsumura, S., Y. Okada, S. Shimada, S. Hori, T. Ohkubo, M. Imoto, M. Ohtake and K. Hamada (1986) : The analyzing system for precursors of earthquakes (APE) of the NRCDP, Japan. Proceedings of the 5th Joint Meeting of the UJNR Panel on Earthquake-Prediction Technology, Tsukuba, Japan.
9) Ohtake, M. and H. Takahashi (1984) : Contribution of the down-hole observation of crustal activity to earthquake prediction. International Symposium on Continental Seismicity and Earthquake Prediction, Beijing, 430-439.
10) Pirhonen, S., F. Ringdal and K. Berteussen (1976) : Event detectability of seismograph stations in Fennoscadia. P.E.P.I., **12**, 329-342.
11) Ringdal, F. (1975) : On the estimation of seismic detection threshold. Bull. Seism. Soc. Am., **65**, 1631-1642.
12) Ringdal, F. (1976) : Maximum-likehood estimation of seismic magnitude. Bull. Seism. Soc. Am., **66**, 789-802.
13) Sato, Y. and D. Skoko (1965) : Optimum distribution of seismic observation points, II. Bull. Earthq. Res. Inst., **43**, 451-457.
14) Shapira, A., O. Kolhanek and R. Wahlstrom (1979) : Detection probabilities for weak regional seismic events. J. Geophy., **46**,123-133.
15) Shapira, A., O. Kulhanek and R. Wahlstrom (1979) : Detectability of regional events by means of the Swedish seismograph station network. Seismological Institute, Uppsala, Report №7-79.
16) Skoko, D., Y. Sato, I. Ochi and T. Dutta (1966) : Accuracy of the determination of earthquake

source parameters as determined by Monte Carlo method. Observation on Indian network. Bull. Earthq. Res. Inst., **44**, 893-900.
17) Ukawa, M., M. Ishida, S. Matsumura and K. Kasahara (1984) : Hypocenter determination method of the Kanto-Tokai observational network for microearthquakes. Research notes of the NRCDP, No.**53**, 88p.
18) Von Seggern, D. and Blandford R. (1976) : Seismic threshold determination. Bull. Seim. Soc Am.,**66**, 753-788.
19) Watanabe, M. (1971) : Determination of earthquake magnitude at regional distance in and near Japan. ZISIN **2**, **24**, 189-200.

(Manuscript Received November 12, 1986)

国立防災科学技術センター地震観測網の震源決定能力及び震源決定精度の調査

ディミトリス・パパナスタシャ*・松村正三**
国立防災科学技術センター

要　旨

国立防災科学技術センターは，関東，東海地域に67箇所の地震観測点を展開している．ここでは，この観測網の震源決定能力及び震源決定精度を調査した．

震源決定能力の評価には，まず個々の観測点毎に，一個の地震を検知し得る確率をマグニチュードと震源距離の関数として表わす．次に，観測網の中で少なくとも3箇所以上の観測点で検知されることを必要条件として，震源が決定され得る確率を求めた．

一方，震源決定精度の評価には，国立科学技術センターの過去の観測データから震源決定精度に関して得られた実際の結果を集計することと，モンテカルロ法を用いて理論的に推測することとの二通りの調査を行い，両者の比較を行った．

この調査には，1984年及び1985年の観測データを使用し，結果は，震源決定可能範囲を示す地図，及び震源決定の誤差に対しての等値線図によって表わした．この結果によると，50kmより浅いM2.0以上の地震であれば観測網内全域でほぼ決定可能，又，M1.5程度の浅い地震の場合は，房総半島に観測の穴が生じていることが解る．精度については，P波到達時刻に標準偏差で0.3秒の誤差が含まれていると仮定して求めた誤差分布が，実際の分布にかなりよく一致していることが解った．

注）ディミトリス・パパナスタシャ氏は，JICAの研修生として来日され，1986年5月より8月までの3ヵ月間，当センターで標記の研究を行われた．同氏は，アテネ国立地震研究所の研究員として，ギリシャでの地震観測網整備の仕事に従事されており，観測網の持つ観測能力の評価法を研究するため来日されたものである．

*アテネ国立地震研究所(ギリシャ)，**国立防災科学技術センター第2研究部